Cellular and nerve regeneration within a biosynthetic extracellular matrix for corneal transplantation

Fengfu Li*†‡, David Carlsson*†‡, Chris Lohmann*§, Erik Suuronen*, Sandy Vascotto*, Karin Kobuch§, Heather Sheardown¶, Rejean Munger*, Masatsugu Nakamura‖, and May Griffith*,

*University of Ottawa Eye Institute, Ottawa, Ontario, Canada K1H 8L6; †National Research Council, Ottawa, Ontario, Canada K1A 0R6; §Universitäts-Augenklinik, University of Regensburg, Regensburg D-93042, Germany; ¶Department of Chemical Engineering, McMaster University, Hamilton, Ontario, Canada L8S 4L7; and ‖Santen Pharmaceutical Company, Ltd., 8916-16 Takayama-cho, Ikoma-Shi 630-0101, Japan

Communicated by Elizabeth D. Hay, Harvard Medical School, Boston, MA, October 20, 2003 (received for review June 9, 2003)

Our objective was to determine whether key properties of extracellular matrix (ECM) macromolecules can be replicated within tissue-engineered biosynthetic matrices to influence cellular properties and behavior. To achieve this, hydrated collagen and *N*-isopropylacrylamide copolymer-based ECMs were fabricated and tested on a corneal model. The structural and immunological simplicity of the cornea and importance of its extensive innervation for optimal functioning makes it an ideal test model. In addition, corneal failure is a clinically significant problem. Matrices were therefore designed to have the optical clarity and the proper dimensions, curvature, and biomechanical properties for use as corneal tissue replacements in transplantation. *In vitro* studies demonstrated that grafting of the laminin adhesion pentapeptide motif, YIGSR, to the hydrogels promoted epithelial stratification and neurite in-growth. Implants into pigs' corneas demonstrated successful *in vivo* regeneration of host corneal epithelium, stroma, and nerves. In particular, functional nerves were observed to rapidly regenerate in implants. By comparison, nerve regeneration in allograft controls was too slow to be observed during the experimental period, consistent with the behavior of human cornea transplants. Other corneal substitutes have been produced and tested, but here we report an implantable matrix that performs as a physiologically functional tissue substitute and not simply as a prosthetic device. These biosynthetic ECM replacements should have applicability to many areas of tissue engineering and regenerative medicine, especially where nerve function is required.

regenerative medicine | tissue engineering | cornea | implantation | innervation

The macromolecules of the extracellular matrix (ECM) are elaborated by cells and create microenvironments that these and other cells will respond to, by differentiating or maintaining their differentiated state. Simulation of appropriate ECM environments within fabricated matrices or scaffolds therefore should encourage parenchymal cells and nerves to infiltrate the matrix, regenerate a structure, and restore key functions to damaged tissues and organs (1). This general tissue engineering (TE) strategy could potentially alleviate problems of organ failure and donor organ shortages for transplantation. To test this strategy, we chose the clinically important regeneration of damaged corneas.

Corneal diseases are a major cause of vision loss, second only to cataracts in overall importance (2), and affect >10 million individuals worldwide (estimates from Vision Share, Raleigh, North Carolina), with corneal scarring from measles being a major cause of childhood blindness (3). Currently, the only widely accepted treatment for corneal blindness is transplantation with human donor tissue. The worldwide demand for transplantation corneas exceeds the supply, and this situation will worsen with an aging population and increased use of corrective laser surgery (4). For patients with disorders such as autoimmune conditions, alkali burns, or recurrent graft failures, corneal transplantation has a poor success rate (5). An alternative for these patients is replacement of the damaged cornea with an artificial substitute. Successful corneal replacement by synthetics is yet to be achieved and existing prostheses neither integrate seamlessly into the host tissue (5), nor promote reinnervation, even though corneal innervation loss can lead to vision loss (6).

The cornea is an avascular, transparent, and immune-privileged tissue comprising three main layers (outer stratified epithelium; stroma of cells networked within a hydrated, mainly collagen–proteoglycan matrix; and inner endothelial layer). The cornea is the main optical element in the eye that refracts light onto the retina for vision and a tough protective barrier for the delicate internal eye tissues. It is one of the most highly innervated tissues in the body (7) and is equipped with nociceptive nerve endings that terminate within the epithelium. These nerve endings are polymodal, mechanosensory, or cold-sensitive (8). Nerve activity is responsible for maintaining overall corneal health, and innervation loss can cause "dry eye" (9), a pathological condition that may result in decreased corneal sensitivity and/or corneal epithelial erosions. When sensitivity is lost, the cornea becomes vulnerable to irreparable injury, ulceration, eventual loss of vision (6), and, in severe cases, blindness (10). The structural and immunological simplicity of the human cornea, and importance of innervation for optimal function, make it an ideal tissue for investigating TE requirements in general and induction of peripheral nerve regeneration in particular.

Our objective was to evaluate novel combinations of biological and synthetic mimics of ECM macromolecules that could be fabricated into TE matrix replacements or tissue templates. By using corneal tissue as the test system, we report here the successful growth of stratified epithelium, stromal fibroblasts, and nerve infiltration with our optically clear ECM substitutes and the successful postsurgical integration of these substitutes into surrounding host tissues of micropig animal models with rapid nerve regeneration.

Materials and Methods

Collagen–Copolymer ECM Replacements. A copolymer [poly(*N*-isopropylacrylamide-coacrylic acid-coacryloxysuccinimide), PNiPAAm-coAAc-coASI, designated TERP] was synthesized by free radical copolymerization of its three monomers (Polysciences) in dioxane. The monomer molar equivalent ratio in the purified TERP was 84.2:9.8:6 by proton NMR in tetrahydrofuran-D_8. The number and weight average molecular mass were 5.6×10^4 and 9×10^4 Da, respectively, as determined by gel permeation chromatography. After purification and solution in PBS, the cloud point was >55°C. Acryloxysuccinimide groups

Abbreviations: ECM, extracellular matrix; LKP, lamellar keratoplasty; TE, tissue engineering.

‡F.L. and D.C. contributed equally to this work.

**To whom correspondence should be addressed. E-mail: mgriffith@ohri.ca.

www.pnas.org/cgi/doi/10.1073/pnas.2536767100

spontaneously crosslink proteins and anchor peptides through their primary amine groups (11). A second copolymer (designated TERP5) was synthesized from TERP by reacting some of its acryloxysuccinimide groups with the peptide YIGSR (YIGSR-NH_2, Nova Biochem, Laufelfingen, Switzerland) in *N*,*N*-dimethyl formamide (48 h at 21°C). The YIGSR peptide is a well known cell adhesion mediator that promotes epithelial growth (12) and enhances neurite extension (13). Collagen–TERP and collagen–TERP5 hydrogels were prepared by mixing neutralized 4% (wt/wt) bovine atelocollagen [1.2 ml; concentrated from 0.3% (wt/vol) collagen; Becton Dickinson], with each purified copolymer (collagen/copolymer = 1.4:1, wt/wt) at 4°C. Each cold solution was injected into plastic contact lens molds, where it reacted at 21°C and then 37°C at 100% humidity to give crosslinked hydrogels of controlled thicknesses. Unreacted acryloxysuccinimide groups in these hydrogels were terminated by immersion in 0.5% (wt/vol) glycine in PBS. Reaction products were extracted and hydrogels sterilized with 1% (wt/vol) chloroform in PBS. YIGSR-NH_2 content of extensively washed gels was 4.3×10^{-11} mol/ml hydrated gel (2.6×10^{-8} g/ml), based on ^{125}I-labeled YIGSR-NH_2 by using the Iodogen method (14). The final total polymer concentration in each hydrated, PBS-equilibrated hydrogel was 3.4% (wt/vol) [collagen and TERP5 at 2 and 1.4% (wt/vol), respectively]. Collagen alone was also neutralized and cast in the same molds and then incubated, first for 24 h at 21°C and then at 37°C, to spontaneously form thermogel controls.

The permeability coefficient of glucose in PBS (pH 7.4) through collagen–copolymer hydrogels was calculated from permeability measurements after enzymatic conversion of glucose to glucose-6-phosphate followed by production of dinucleotide quantified by its UV absorption (15). Topographies of hydrogels in PBS were examined by atomic force microscopy (Molecular Imaging, Tempe, AZ) in the "contact" mode. Pore sizes from this technique were compared with average pore diameters calculated from PBS permeability (13). Implants recovered after 6 wk *in vivo* were examined by IR spectroscopy (Midac M, Fourier transform IR spectrometer, ZnSe beam condenser, and diamond cell).

***In Vitro* Characterization.** Immortalized corneal epithelial cells (16) were used to evaluate epithelial coverage. Collagen, collagen–TERP, and collagen–TERP5 hydrogels (500 μm thick for easy handling) were embedded separately on top of a collagen-based matrix that consisted of a mixture of blended neutralized type I rat-tail tendon collagen (0.3%, wt/vol; Becton Dickinson) and chondroitin 6-sulfate (1:5, wt/wt), crosslinked with 0.02% (vol/vol) glutaraldehyde (followed by glycine termination of unreacted aldehyde groups) and then thermogelled at 37°C. Epithelial cells were seeded on top, and constructs were supplemented with epidermal growth factor-containing keratinocyte serum-free medium (Life Technologies) until confluence. The medium was then switched to a serum-containing medium (modified supplemental hormone epithelial media; ref. 17) for 2 d, followed by maintenance at an air–liquid interface. At 2 wk, constructs were fixed in 4% paraformaldehyde in 0.1 M PBS and were processed for routine hematoxylin and eosin staining. The number of cell layers and thickness of the epithelium were measured from six random areas for each of four samples within each of the three experimental groups of hydrogels.

Other constructs, as above, were used to examine early nerve in-growth. Dorsal root ganglia from 8-d-old chick embryos were embedded within the surrounding matrix adjacent to each implant. Cultures were supplemented with keratinocyte serum-free medium containing 2% B27 and 1% N2 supplements (Life Technologies) and 1 nM retinal acetate (Sigma). After 4 d, constructs were fixed as described above for immunohistochemistry on whole mounts (details below) to visualize construct innervation. Nerve density (the number of nerves per μm^2) was calculated at distances of 75 and 100 μm from the edge of the dorsal root ganglia within a 90° pie-shaped wedge extending into the implant.

Implantation and Clinical Evaluation. Following the Association for Research in Vision and Ophthalmology animal use guidelines, six identical collagen–TERP5 matrices (5.5 mm in diameter, 200 ± 50 μm thick) were implanted into the right corneas of six Yucatan micropigs (Charles River Breeding Laboratories) by lamellar keratoplasty (LKP). Contralateral unoperated corneas served as controls. A further four pigs received allografts of fresh pig donor corneas with the same dimensions as TERP5 matrices, implanted by LKP.

Briefly, in LKP, under general anesthesia, a 250-μm-deep, 5-mm-diameter circular incision was made by using a Barraquer trephine (Geuder, Heidelberg). A lamellar dissection was then performed by using a microsurgical pocket blade (Geuder) along a natural uniform stratum in the corneal stroma to remove host epithelium and anterior stroma. Tissue removed was replaced with an implant 0.5 mm larger in diameter to allow adequate wound apposition between graft and host tissue. The host's posterior stroma, Descemet's membrane, and endothelium remained. For three implants and four allografts, after surgery, an amniotic membrane was sutured over the entire corneal surface for 7 d to keep implants in place. In another three animals, collagen–TERP5 implants were sutured into the host tissue by using eight interrupted 10–0 nylon sutures. Postoperative medication consisted of dexamethasone and gentamycin four times daily for 21 d.

Pigs were examined daily for 7 d after the operation and then weekly. Examinations included slit-lamp assessment of corneal optical clarity, sodium fluorescein staining to assess epithelial integrity and barrier function (18), intraocular pressure measurements to ensure appropriate aqueous humor flow, and *in vivo* confocal microscopy with a ConfoScan microscope (Nidek, Erlangen, Germany) to assess cell and nerve in-growth. For *in vivo* confocal microscopy, light scattering at the graft-host tissue interphase marked the implant boundaries. *Z* scans were taken and nerves were qualified as stromal when they were embedded in the corneal stroma (keratocytes above and below nerves) and as subepithelial when nerves were directly under the epithelium. Corneal touch sensitivity was measured by using a Cochet–Bonnet esthesiometer (Handaya, Tokyo) at five points within the implant area of each cornea, as described (19). In brief, a fine filament was extended from this tool to contact the cornea and reflex responses of the pig were monitored. Initially, very soft contact was made by using a long filament extension, which was then shortened progressively (becoming stiffer and the touch firmer) until the pig clearly responded. This extension was recorded as the touch-sensitivity threshold.

Immunohistochemistry and Histopathological Examination. Tissues and constructs were fixed in 4% paraformaldehyde in 0.1 M PBS. For nerve immunolocalization, flat mounts were permeabilized with a detergent mixture (20) (150 mM NaCl/1 mM ethylenediamine tetraacetic acid/50 mM Tris/1% Nonidet P-40/0.5% sodium deoxycholate/0.1% SDS), blocked for nonspecific staining with 4% FCS in PBS, and incubated in antineurofilament 200 Ab (Sigma). They were then incubated with FITC or Cy3-conjugated secondary Abs (Sigma and Amersham Biosciences, respectively) and visualized by confocal microscopy.

For histology and further immunohistochemistry, samples were paraffin embedded and sectioned. Sections were hematoxylin- and eosin-stained for histopathological examination. Immunofluorescence was performed as described above on deparaffinized sections for expression of type VII collagen (Sigma), a hemidesmosome complex marker (in anchoring fibrils) (21).

Immunohistochemical staining using peroxidase-diaminobenzidine visualization was performed with the following: AE1/AE3 Ab (Chemicon) for epithelial markers, anti-vimentin Ab (Roche) for stromal fibroblasts, antismooth muscle actin Ab, 1A4 (Cell Marque, Austin, TX) for activated stromal fibroblasts (myofibroblasts), and SP1-D8 Ab (Developmental Studies Hybridoma Bank, Iowa City, IA) for procollagen 1 synthesis (to localize sites of *de novo* collagen synthesis). CD15 and CD45 staining for immune cells (Becton Dickinson) was performed by using the ARK peroxidase kit (DAKO) to preconjugate the primary Abs to their respective secondary Abs and peroxidase for visualization. For anti-vimentin, anti-smooth muscle actin, and SP8-D1 Abs, antigen retrieval was preformed by pretreating with proteinase K (2 mg/ml) for 30 min at 37°C before incubation in primary Ab. *Ulex europaeus agglutinin* lectin staining was used to visualize tear film mucin deposition (22). Samples were incubated with biotinylated *Ulex europaeus agglutinin* (Sigma) and then reacted with avidin-horseradish peroxidase and visualized with diaminobenzidine. For transmission electron microscopy, all samples were treated in conventional fixative, stain, and potting resin (Karnovsky's fixative/OsO_4/uranyl acetate/epoxy).

Results

Collagen–Copolymer Implants. Hydrogels were prepared from atelocollagen crosslinked with TERP or its YIGSR-modified analog, TERP5. Based on ^{125}I labeling, water-insoluble collagen–TERP5 hydrogels contained 60% of the YIGSR-NH_2 expected from the TERP5 composition (Fig. 1*A*) after exhaustive aqueous extraction. IR spectroscopy showed progressive loss of oxysuccinimide groups during reaction of TERP and TERP5 with collagen, consistent with the expected crosslinking reaction (11). The composite collagen–copolymer matrices, molded to the curvature and dimensions of a cornea (Fig. 3*B*), were adequately robust and suturable and had refractive indices (1.343 ± 0.003) comparable with the human tear film (1.336–1.357; ref. 23). They showed high optical clarity compared to collagen-only matrices (Fig. 1 *B* and *C*) with direct transmission and backscatter of visible light superior to human corneas. The collagen–copolymer matrices had pore diameters of 140–190 nm (from both atomic force microscopy and PBS permeability; ref. 13). They also had a glucose diffusion permeability coefficient of 2.7×10^{-6} cm^2/s, higher than the value for natural stroma [$\approx 0.7 \times 10^{-6}$ cm^2/s, from published diffusion (2.4×10^{-6} cm^2/s) and solubility (0.3) coefficients (24)].

***In Vitro* Tests Matrices.** The epithelium on collagen–TERP5 hydrogels had a significantly greater number of cell layers (Fig. 1*D*) and was thicker (Fig. 1 *E–G*) than collagen–TERP or collagen-only hydrogels. The density of nerves growing into collagen–TERP5 matrices (Fig. 1*E*) was significantly higher than that into collagen matrices. Only nerves grown in collagen–TERP5 hydrogels reached 100 μm from the edge of the matrix, but this trend for collagen–TERP5 polymer to support longer nerves was not statistically significant compared with collagen–TERP. Nevertheless, these results established collagen–TERP5 hydrogel as the superior candidate in supporting cell growth, and only this hydrogel matrix was used as an implant for the *in vivo* studies. Collagen-only gels were too weak to suture, were opaque, and had poor epithelial overgrowth and nerve in-growth (Fig. 1).

Regeneration After Biosynthetic Matrix Implantation. Collagen-TERP5 matrices were suturable with careful surgical manipulation (Fig. 2 *A–C*), with no indication of cracking or cutting by sutures. As with control allografted corneas, intraocular pressures were 10–14 mmHg (1 mmHg = 133 Pa) preoperatively, and 10–16 mmHg postoperatively over the 6-wk study period, showing that the implants did not block aqueous humor flow within

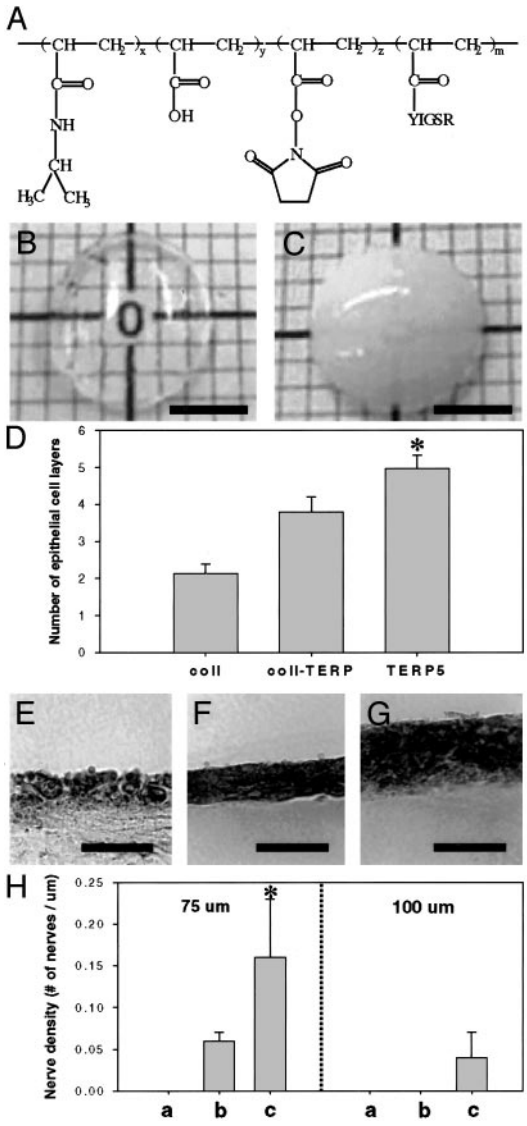

Fig. 1. Biosynthetic matrices *in vitro*. (*A*) Structure of TERP5 copolymer (x/y/z/m = 84.2:9.8:6:5 × 10^{-5}, all in molar equivalents). (*B*) Corneal implant comprising collagen–TERP5 hydrogel, showing optical clarity that was not achieved in matrices containing only collagen (*C*). (Bar = 5 mm, thickness = 500 μm in both cases.) (*D*) Number of cell layers within the stratified epithelium grown on different hydrogels, $n = 4$ samples each. *, $P < 0.05$ by ANOVA. (*E–G*) Thickness of the epithelium grown on different hydrogels: collagen only (*E*), collagen–TERP (*F*), and collagen–TERP5 (*G*). (Bar = 30 μm for *E–G*.) (*H*) Nerve density within different hydrogels (collagen, a; collagen–TERP, b; collagen–TERP5, c) at 75 and 100 μm from the hydrogel edge, n = three samples each. *, $P < 0.05$ vs. collagen by ANOVA.

the eye. Neither implants nor allografts gave adverse inflammatory or immune reaction, and both remained optically clear. By 4–5 d postoperative, both implants and allografted corneas were covered with epithelium. By 1 wk, sodium fluorescein dye was excluded, indicating that the epithelium was intact and had reestablished barrier properties. Stratified epithelium remained intact (excluded fluorescein) and firmly attached (as indicated by wiping a Weck sponge over the epithelial surface during clinical examinations) over the entire 6 wk. Clinical *in vivo* confocal microscopy of implanted stromal matrices at 3 wk after surgery showed a regenerated epithelium (Fig. 2*D*), newly in-grown nerves (Fig. 2*G*), and stromal (Fig. 2*J*) and endothelial cells (Fig. 2*M*) with cellular morphology mimicking that of

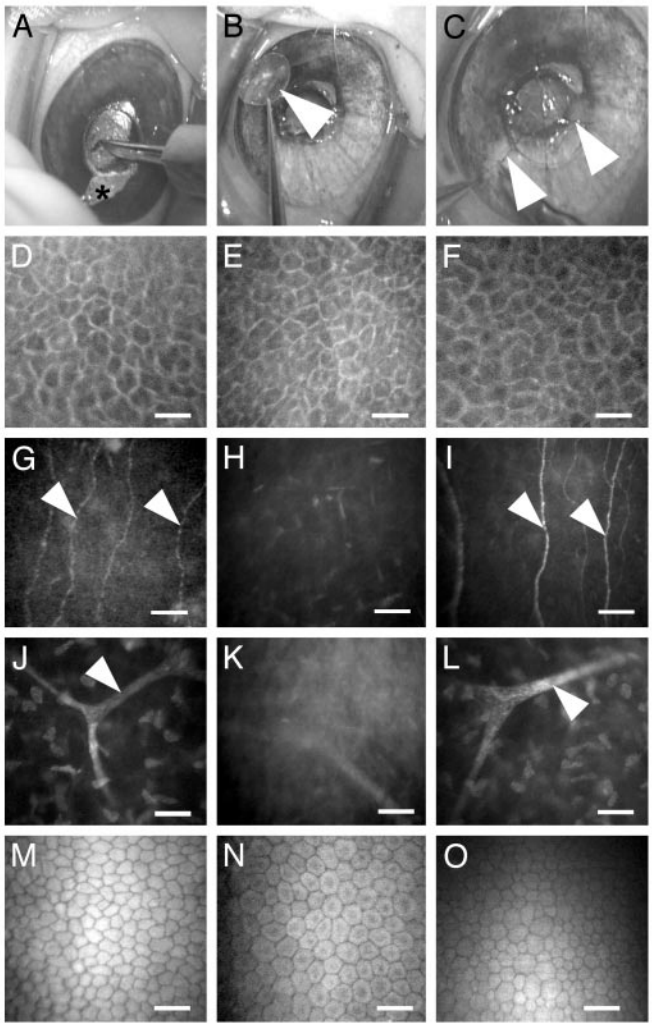

Fig. 2. Corneal implantation by LKP and *in vivo* confocal microscopic images of 6-wk implants. (*A–C*) LKP procedure on a Yucatan micropig. (*A*) A trephine is used to cut a circular incision of preset depth into the cornea. Anterior corneal layers are removed (*B*) and replaced with a biosynthetic implant (arrow), which is sutured in place (*C*). Arrowheads indicate sutures. (*D*) *In vivo* confocal image showing regenerated corneal epithelium on implant surface. Corresponding allograft control (*E*) contains donor epithelium, whereas the unoperated control (*F*) has intact epithelium. Regenerated nerves (arrowheads) at the interface between implant and overlying regenerated epithelium (*G*) correspond to the subepithelial nerves in the unoperated control (*I*). (*H*) In the allograft, however, subepithelial nerves are absent. (*J–L*) Stromal cells and branching nerve bundle (arrowhead) deeper within the underlying stroma of corneas with implant (*J*) and allograft (*K*) and in a corresponding region in the control (*L*). (*M–O*) The endothelium in corneas with implant (*M*), allograft (*N*), and unoperated controls (*O*) are intact and show similar morphology. (Bar = 25 μm for *D–F* and 5 μm for *G–O*.)

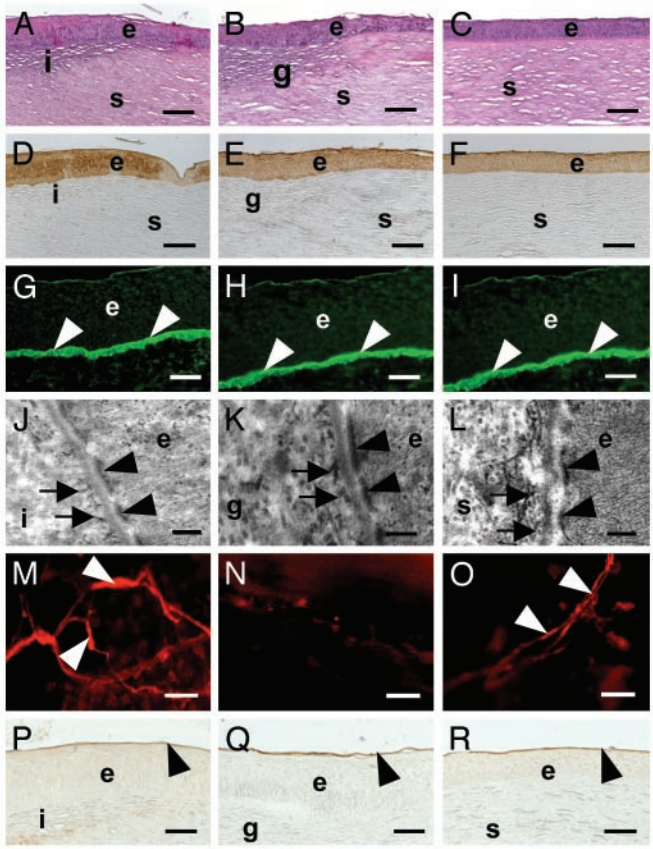

Fig. 3. Postsurgical corneal regeneration. (*A–C*) Hematoxylin- and eosin-stained sections showing stromal cells in implant (*A*) and allograft control (*B*). Both appear to be seamlessly integrated into the host. (*C*) Unoperated control. (*D–F*) Positive AE1/AE3 cytokeratin Ab staining in regenerated epithelium overlying implant (*D*), which is similar to epithelium of allograft (*E*) and unoperated control (*F*). (*G–I*) Immunolocalization of type VII collagen, a marker for hemidesmosomes, at the epithelium–implant interface (arrows) in the implant (*G*), allograft (*H*), and control (*I*). (*J–L*) Transmission electron microscopy of epithelium–implant interface. Hemidesmosome plaques (arrowheads) and anchoring fibrils (arrows) have formed within the ECM between the epithelial cells and underlying implant (*J*), emulating the structures normally found at the epithelial–stromal interface as demonstrated in the allograft (*K*) and control (*L*). Flat mount of cornea shows nerve fibers (arrows) within the implant (*M*) and unoperated control (*O*), but not in the allograft (*N*), stained with an antineurofilament Ab. *Ulex europaeus agglutinin* binding (arrowheads) to the epithelial surface on the implant (*P*) and allograft (*Q*) indicate restoration of tear film mucin layer in all cases. (*R*) Unoperated control. e, epithelium; i, implant; g, allograft; s, stroma. (Bar = 100 μm for *A–F*, 40 μm for *G–I*, 200 nm for *J–L*, 20 μm for *M–O*, and 30 μm for *P–R*.)

unoperated controls (Fig. 2 *F*, *I*, *L*, and *O*). Epithelial and endothelial cell morphology in the allografts (Fig. 2 *E* and *N*) resembled that of untreated controls. However, subepithelial and stromal nerves were not observed at 3 (Fig. 2 *H* and *K*) or 6 wk after surgery.

Implants that recovered after 6 wk *in vivo* had IR spectra clearly indicating the presence of the copolymer. Histological sections through corneas with implants showed a distinct but smooth implant–host tissue interface (Fig. 3*A*) resembling that of control corneas with allografts (Fig. 3*B*). In both corneas with implants or allografts, the regenerated epithelium was stratified with no significant difference in epithelial thickness between treatments ($P < 0.05$). Detailed examination showed a fully differentiated epithelium that was positively stained by AE1/AE3 Ab markers (Fig. 3 *D* and *E*), overlying a regenerated basement membrane that was positive for type VII collagen, a marker for hemidesmosomes (21) at the basement membrane–epithelium interface (Fig. 3 *G* and *H*). Transmission electron microscopy observations indicated morphology consistent with the presence of hemidesmosomes (Fig. 3 *J* and *K*). In implants, neurofilament-positive in-growing nerves had begun to reestablish a subepithelial network and showed extension into the epithelial cells (Fig. 3*M*). No subepithelial nerves were located in the allografted corneas (Fig. 3*N*). The mucin layer of the tear film was restored in corneas with implants (Fig. 3*P*) as in the allograft (Fig. 3*Q*).

Immunohistochemistry indicated that cells within both implant and allograft were synthesizing procollagen I. However,

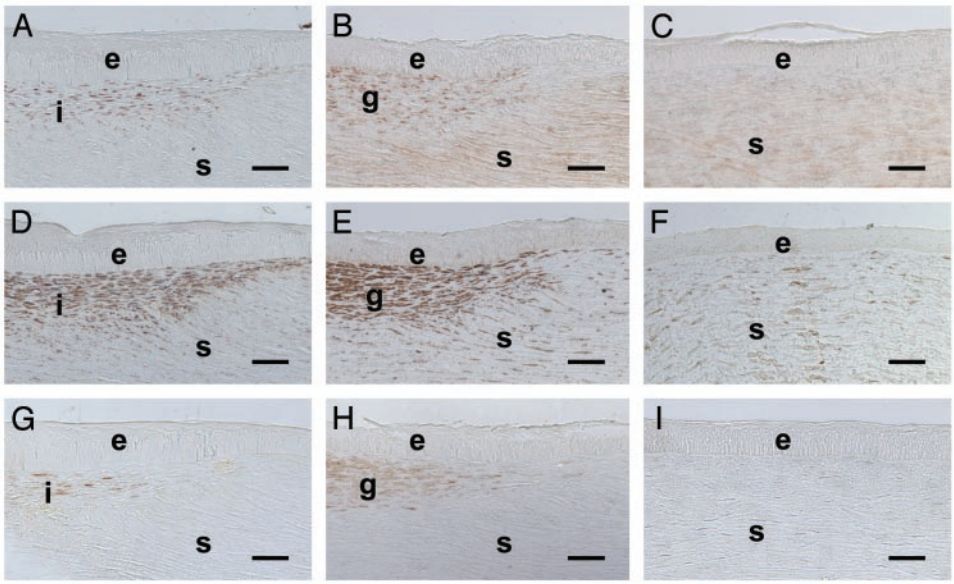

Fig. 4. Implant–host integration at 6 wk after surgery. (*A–C*) Staining for procollagen type I. Positive staining is observed in matrix of both the implanted hydrogel (*A*) and the allograft control (*B*), indicating sites of new collagen deposition. (*C*) Unoperated control has no new collagen synthesis. (*D–F*) Staining for vimentin throughout stroma identifies stromal fibroblasts. Staining throughout the implanted hydrogel (*D*) demonstrates cell invasion. Cells may also been seen within the implanted allograft (*E*) and throughout the unoperated control (*F*). (*G–I*) Smooth muscle actin staining indicates activated myofibroblasts and the potential for scarring. In the hydrogel implant (*G*), staining is occasionally present in the hydrogel but is not found in the host stroma or the transition zone between host and implant. Positive staining in the allograft-implanted cornea (*H*) is identified in both the allograft and the transition zone but not the intact host stroma. (*I*) Unoperated control. e, epithelium; i, implant; g, allograft; s, stroma. (Bar = 100 μm in all cases.)

more procollagen synthesis occurred in the allografts as indicated by more intense staining in allografts compared to implants (Fig. 4 *G* and *H*). Both allografts and implants had vimentin-positive stromal cells (no statistically significant difference between groups, $P < 0.05$; Fig. 4 *A* and *B*), indicating a fibroblastic phenotype. Both also showed smooth muscle actin staining and therefore the presence of activated stromal fibroblasts, with no statistically significant difference in positive cell counts ($P < 0.05$; Fig. 4 *D* and *E*).

Corneal touch sensitivity, measured pre- and postoperatively by esthesiometry (19), showed a dramatic drop in touch sensitivity after surgery. However, recovery of sensitivity occurred between 7 and 14 d, and by 21 d postoperative had returned to preoperative levels (Fig. 5). In control animals that had received donor corneal allografts, however, the corneas remained anesthetic over the 6-wk period (Fig. 5).

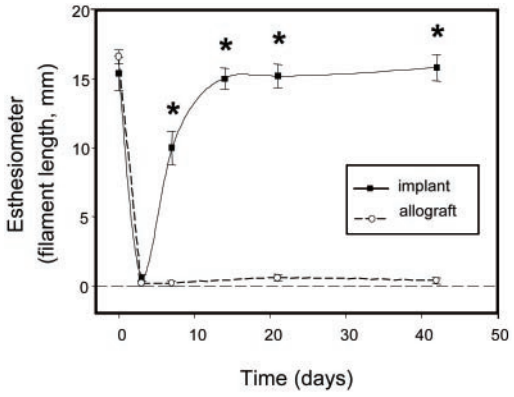

Fig. 5. Corneal touch sensitivity in implants vs. allografts by esthesiometry. All groups, $n = 3$. *, $P < 0.01$ by repeated-measures ANOVA with Tukey two-way comparisons.

Discussion

The human cornea comprises ≈70% dry weight type I collagen (25). Other ECM molecules present include primarily smaller keratin sulfate proteoglycans that form intercollagen linkages. During natural corneal development, cellular secretions and ECM sequesterization produces microenvironments that dictate later functions (26). Our corneal ECM replacement was designed to mimic natural ECM characteristics by containing collagen and emulating the natural crosslinks with TERP5 copolymer synthesized from *N*-isopropylacrylamide. Such polymers are well known to allow cell growth on their surface (27) and, more importantly, when cells are completely encapsulated (28). TERP5 contained grafted YIGSR and also spontaneously reacted with ε-NH_2 groups of collagen at neutral pH to form gels at 21°C. This resulted in collagen becoming locked in a form with microfibril diameters well below the wavelengths of visible light. This is critical for optical clarity (29) and similar to the human cornea (30). The crosslinking reaction allowed us to take advantage of the cell growth promoting and chemotrophic properties inherent to collagen and the laminin YIGSR peptide, an established cell adhesion mediator and promoter of epithelial growth (12) and enhancer of neurite extension (13), as well as the propensity of the "rigid rod" collagen backbone to form robust hydrogels. Our hydrogel matrices were less robust than the highly regular human corneal ECM (30), probably because they were random arrays of rigid rod collagen chains, but were adequate for suturing.

We removed and replaced only the more superficial portion of the cornea (epithelium and anterior stroma) by LKP, a surgical procedure used to treat patients whose more superficial portions of the corneal are damaged. Nonpenetration of the anterior chamber keeps the inner contents of the eye intact and reduces the rate of rejection and postoperative complications (e.g., infection), thus improving long-term graft stability (31) and in this study, eliminates the potential confounding factor of postsurgical infection. Our collagen—TERP5 matrix replacements

were designed with the goal of promoting host tissue repair and regeneration by allowing in-growth of host corneal cells and nerves. Nerve regrowth into these biosynthetic composites occurred within 3 wk of surgery in micropigs, as found in wounded rabbit corneas (32). Touch sensitivity was also restored within the same time frame, although no nerve regrowth or touch sensitivity was observed in corneas of pigs that received allografts. Here, traditional allografts containing donor cells were used, as is the case of human corneal transplantations that the implants are designed to replace. This corresponds to reports where nerve in-growth and touch sensitivity recovers slowly (>18 mo after laser refractive eye surgery; >10 yr after LKP) after human corneal wounding or transplantation (33, 34). Our result, therefore, represents a dramatic advance over the slow nerve regeneration after current human donor allograft therapy (34) and a demonstration of *in vivo* nerve regeneration in the cornea promoted by a fabricated material.

Implants recovered after 6 wk *in vivo* had IR spectra, clearly indicating the presence of copolymer scaffold in regions showing cell and nerve in-growth and that were tested for touch sensitivity. Although the hematoxylin and eosin demarcates a continuous transition between polymer and host, this was most likely caused by stromal cell in-growth (Fig. 4*D*). The low level of smooth muscle actin indicates a limited conversion of stromal cells into activated myofibroblast-like cells, which might produce opacity (by scarring, causing light scatter). Overall, the ECM replacements were able to emulate key properties of natural ECM macromolecules by (*i*) allowing for cell-matrix interaction in the restoration of functional structures including the generation of a basement membrane between the implant and overlying epithelium, stromal cell, and nerve axon ingrowth; (*ii*) potentiating the differentiated cell state; and (*iii*) integrating into the host tissue. Finally, this concept of emulating a natural ECM to stabilize a damaged tissue and allowing for regeneration makes the TE polymer implant distinct from current prosthetic cornea strategies (5).

Overall, we can now control the strength and optical clarity of noncytotoxic, biosynthetic composites to the point that TE corneal replacements may, ultimately, address future world shortages of donor corneas. In addition, such corneal implants could circumvent potential problems resulting from the lack of nerve regeneration after surgery, found both in human donor tissue (34, 35) and in other proposed, fully synthetic, or acylated collagen implants (5, 36). These biosynthetic matrices with bound cell adhesion factors may have implications for the general field of tissue engineering, especially for the challenging problem of nerve regeneration and the innervation of other engineered organ and tissue systems.

We thank Drs. S. Shimmura, W. Hodge, G. Mintsioulis, and R. Worton for helpful insights. This work was supported by Natural Sciences and Engineering Research Council Canada Grants 227212-99, 227951-01, and 246418 and an International Foundation for Ethical Research studentship for *in vitro* work (E.J.S.).

1. Chapekar, M. S. (2000) *J. Biomed. Mater. Res.* **53,** 617–620.
2. Whitcher, J. P., Srinivasan, M. & Upadhyay, M. P. (2001) *Bull. W. H. O.* **79,** 214–221.
3. Gilbert, C. & Foster, A. (2001) *Bull. W. H. O.* **79,** 227–232.
4. Eye Bank Association of America (1999) *Eye Banking Statistical Report* (Eye Bank Assoc. Am., Washington, DC).
5. Chirila, T. V. (2001) *Biomaterials* **22,** 3311–3317.
6. Lambiase, A., Rama, P., Bonini, S., Caprioglio, G. & Aloe, L. (1998) *N. Engl. J. Med.* **338,** 1174–1180.
7. Rozsa, J. & Beuerman, R. W. (1982) *Pain* **14,** 105–120.
8. Gallar, J., Pozo, M. A., Tuckett, R. P. & Belmonte, C. (1993) *J. Physiol. (London)* **468,** 609–622.
9. Stern, M. E., Beuerman, R. W., Fox, R. I., Gao, J., Mircheff, A. K. & Pflugfelder, S. C. (1998) *Adv. Exp. Med. Biol.* **438,** 643–651.
10. Gilbard, J. P. & Rossi, S. R. (1990) *Ophthalmology* **97,** 308–312.
11. Pollak, A., Blumenfeld, H., Wax, M., Baughn, R. L. & Whitesides, G. M. (1980) *J. Am. Chem. Soc.* **102,** 6324–6336.
12. Graf, J., Ogle, R. C., Robey, F. A., Sasaki, M., Martin, G. R., Yamada, Y. & Kleinman, H. K. (1987) *Biochemistry* **26,** 6896–6900.
13. Bellamkonda, R., Ranieri, J. P. & Aebischer, P. (1995) *J. Neurosci. Res.* **41,** 501–509.
14. Aucoin, L., Griffith, C. M., Pleizier, G., Deslandes, Y. & Sheardown, H. (2002) *J. Biomater. Sci. Polym. Ed.* **13,** 447–462.
15. Bondar, R. J. & Mead, D. C. (1974) *Clin. Chem.* **20,** 586–590.
16. Araki-Sasaki, K., Aizawa, S., Hiramoto, M., Nakamura, M., Iwase, O., Nakata, K., Sasaki, Y., Mano, T., Handa, H. & Tano, Y. (2000) *J. Cell. Physiol.* **182,** 189–195.
17. Jumblatt, M. M. & Neufeld, A. H. (1983) *Invest. Ophthalmol. Visual Sci.* **24,** 1139–1143.
18. Josephson, J. E. & Caffery, B. E. (1988) *Invest. Ophthalmol. Visual Sci.* **29,** 1096–1099.
19. Millodot, M. (1984) *Ophthal. Physiol. Opt.* **4,** 305–318.
20. Brugge, J. S. & Erikson, R. L. (1977) *Nature* **269,** 346–348.
21. Gipson, I. K., Spurr-Michaud, S. J. & Tisdale, A. S. (1988) *Dev. Biol.* **126,** 253–262.
22. Shatos, M. A., Rios, J. D., Tepavcevic, V., Kano, H., Hodges, R. & Dartt, D. A. (2001) *Invest. Ophthalmol. Visual Sci.* **42,** 1455–1464.
23. Patel, S., Marshall, J. & Fitzke, F. W., III (1995) *J. Refract. Surg.* **11,** 100–105.
24. McCarey, B. E. & Schmidt, F. H. (1990) *Curr. Eye Res.* **9,** 1025–1039.
25. Lisenmeyer, T. F. (1981) in *Cell Biology of the Extracellular Matrix* (Plenum, New York), pp. 5–37.
26. Hay, E. D. (1980) *Curr. Top. Dev. Biol.* **14,** 359–370.
27. Yamato, M., Utsumi, M., Kushida, A. I., Konno, C., Kikuchi, A. & Okano, T. (2001) *Tissue Eng.* **7,** 473–480.
28. Stile, R. A., Burghardt, W. R. & Healy, K. E. (1999) *Macromolecules* **32,** 7370–7379.
29. Freegard, T. J. (1997) *Eye* **11,** 465–471.
30. Meller, D., Peters, K. & Meller, K. (1997) *Cell Tissue Res.* **288,** 111–118.
31. Terry, M. A. (2000) *Cornea* **19,** 611–616.
32. Tervo, K., Latvala, T. M. & Tervo, T. M. (1994) *Arch. Ophthalmol.* **112,** 1466–1470.
33. Mathers, W. D., Jester, J. V. & Lemp, M. A. (1988) *Arch. Ophthalmol.* **106,** 210–211.
34. Kaminski, S. L., Biowski, R., Lukas, J. R., Koyuncu, D. & Grabner, G. (2002) *J. Refract. Surg.* **18,** 731–736.
35. Richter, A., Slowik, C., Somodi, S., Vick, H. P. & Guthoff, R. (1996) *Ger. J. Ophthalmol.* **5,** 513–517.
36. Kornmehl, E. W, Bredvik, B. K., Kelman, C. D., Raizman, M. B. & DeVore, D. P. (1995) *J. Refract. Surg.* **11,** 502–506.